

# Detection of Building Response Changes Using Deconvolution Interferometry: A Case Study in Bogota, Colombia

Nathalia Jaimes<sup>1</sup>, Germán A. Prieto<sup>\*1</sup> , and Carlos Rodriguez<sup>2</sup> 

## Abstract

Seismic structural health monitoring allows for the continuous evaluation of engineering structures by monitoring changes in the structural response that can potentially localize associated damage that has occurred. For the first time in Colombia, a permanent and continuous monitoring network has been deployed in a 14-story ecofriendly steel-frame building combined with a reinforced concrete structure in downtown Bogota. The six three-component ETNA-2 accelerometers recorded continuously for 225 days between July 2019 and February 2020. We use deconvolution-based seismic interferometry to calculate the impulse response function (IRF) using earthquake and ambient-vibration data and a stretching technique to estimate velocity variations before and after the  $M_w$  6.0 Mesetas earthquake and its aftershock sequence. A consistent and probably permanent velocity variation (2% reduction) is detected for the building using ambient-vibration data. In contrast, a 10% velocity reduction is observed just after the mainshock using earthquake-based IRFs showing a quick recovery to about 2%. A combination of both earthquake-based and ambient-vibration-based deconvolution interferometry provides a more complete picture of the state of health of engineering structures.

**Cite this article as** Jaimes, N., G. A. Prieto, and C. Rodriguez (2021). Detection of Building Response Changes Using Deconvolution Interferometry: A Case Study in Bogota, Colombia, *Seismol. Res. Lett.* **93**, 931–942, doi: [10.1785/SR202010219](https://doi.org/10.1785/SR202010219).

[Supplemental Material](#)

## Introduction

Continuous evaluations of the state of health of engineering structures (Farrar and Worden, 2010), such as buildings (Mordret *et al.*, 2017; Çelebi, 2019; Rahmani and Todorovska, 2021), bridges (Salvermoser *et al.*, 2015; Kaya and Ventura, 2019), and dams (Bukanya *et al.*, 2014; Planès *et al.*, 2016; Oliveira and Alegre, 2019), are key to obtaining reliable information about the integrity of these structures and ultimately seismic risk. In recent years, new methodologies and data have become available to allow for such continuous monitoring, detection (and location) of damage in buildings using wave propagation approaches (Snieder and Safak, 2006; Todorovska and Trifunac, 2008; Nakata *et al.*, 2015; Massari *et al.*, 2018; Park and Oh, 2018) and sometimes using impulse response functions (IRFs) (e.g., Mordret *et al.*, 2017) or fitting beam-type or finite-element models for structural system identification (Ebrahimian and Todorovska, 2015; Sun *et al.*, 2017) to study the effects of environmental variables (Nakata and Snieder, 2014; Sun *et al.*, 2017) or extreme events such as earthquakes (Kohler *et al.*, 2007; Nakata *et al.*, 2013). Buildings can be damaged due to exposure to environmental continuous deterioration and unexpected natural disasters, such as earthquakes. In this regard, structural health monitoring (SHM) technology has been actively developed to ensure the safety of buildings (Park and Oh, 2018).

Snieder and Safak (2006) proposed a deconvolution-based seismic interferometry approach to separate the IRF of the building from the source of excitation and from the soil-structure interaction, instead of a correlation-based approach (Snieder *et al.*, 2009; Wen and Kalkan, 2017). Estimating the IRF between different floors is possible using earthquake records (Snieder and Safak, 2006; Kohler *et al.*, 2007; Todorovska and Trifunac, 2008; Nakata *et al.*, 2013, 2015) or ambient vibrations (Prieto *et al.*, 2010; Nakata and Snieder, 2014; Sun *et al.*, 2017). Earthquake-based IRFs can be obtained using very short-time windows and can be used to detect response changes at very short-time scales (Todorovska and Trifunac, 2008), whereas using ambient vibrations can provide a continuous picture (not possible using earthquakes, especially in regions with little earthquake activity) of the building response and has been applied in a wide range of monitoring purposes including volcanos (Sens-Schönferder and Wegler, 2006; Brenguier, Shapiro, *et al.*, 2008; Obermann *et al.*,

1. Departamento de Geociencias, Universidad Nacional de Colombia, Bogotá, Colombia,  <https://orcid.org/0000-0001-8538-7379> (GAP); 2. Universidad ECCI, Bogotá, Colombia,  <https://orcid.org/0000-0002-8666-6377> (CR)

\*Corresponding author: [gaprietogo@unal.edu.co](mailto:gaprietogo@unal.edu.co)

© Seismological Society of America

2013), fault zones (Brenguier, Campillo, *et al.*, 2008), subduction areas (Ikeda and Tsuji, 2018), slope stability in massive rock structures (Cárdenas-Soto *et al.*, 2016), and much more.

Based on the estimated IRFs, a number of approaches have been used for studying the temporal variations of wave velocities in buildings. One approach uses the IRF arrival times between two floors by visual inspection, for example, between the ground level and various floors or from the top floor to lower levels (e.g., Todorovska and Trifunac, 2008; Nakata *et al.*, 2013). Another approach uses a numerical model with a limited number of unknown parameters that describe the building to match the predicted and observed IRFs (Ebrahimian and Todorovska, 2015; Sun *et al.*, 2017; Rahmani and Todorovska, 2021). A recent approach takes advantage of coda-wave interferometry monitoring approaches in seismology (Snieder *et al.*, 2002; Brenguier, Shapiro, *et al.*, 2008) in which the IRFs at two different times are compared using waveform coherence (or cross correlations) to extract relative time delays with the time axis of one trace being stretched or compressed to obtain the best correlation with the other trace (Sens-Schönfelder and Wegler, 2006; Mordret *et al.*, 2017).

In this contribution, we use deconvolution-based interferometry using both earthquake and ambient-vibration data to study velocity variations over a period of 224 days in a building in downtown Bogota, Colombia. During the recorded period, an  $M_1$  6.0 earthquake occurred about 150 km east of Bogota followed by an  $M_1$  5.8 aftershock that produced significant changes in the building response.

## Data and Methods

The Crisanto Luque is a 14-story building with a steel frame combined with a reinforced concrete structure located in downtown Bogota, Colombia. The six three-component ETNA-2 accelerometers were installed, one located in the basement of the building and the others in the second, fifth, eighth, 11th, and 14th floors (ceiling). The instruments record at 200 samples per second continuously starting June 2019, although continuous recording halted in February 2020. The sensor on the ceiling used a Global Positioning System (GPS) clock, and timing for the other sensors was obtained through network timing protocol using the building's ethernet network. The Ycomponent of the fifth floor sensor was also unresponsive. This is, as far as we know, the longest SHM experiment in Colombia. This building array provides an excellent data set to study temporal variations of building response to natural and anthropogenic sources (see [Data and Resources](#)).

Here, we analyze 225 days (between 3 July 2019 and 14 February 2020) of continuous recording on both horizontal components of the sensors. Sensors are located along the southeast side of the rectangular-shaped building as shown in Figure 1. The sensors were bolted to the floor of the building, except for the sensor in the ceiling (14th floor), which was bolted to the ceiling, to enable the GPS to have a view of the sky.

Figure 2 shows example amplitude spectrograms of the 14th floor, where the general behavior of anthropogenic sources is evident with higher amplitudes during business hours and lower amplitudes at night (corresponding traces shown in Fig. S1, available in the supplemental material to this article). Detected earthquakes are present, the most obvious being an  $M_1$  6.0 earthquake and its early aftershocks. The main modes of vibration of the building include 1.25 Hz, overtones at 2.37 and 3.13 Hz, and a prominent mode at 3.9 Hz (a similar figure for the Y component is shown in Fig. S2). Because our main objective is not mode and mode shape estimation, no further analysis of the modes is discussed, and it is left for future research.

From the continuous data available between July 2019 (2019-184) and February 2020 (2020-044), a total of 49 earthquakes with  $M_1 > 3.5$  were used in this study for monitoring purposes (see Table S1). Most of these earthquakes (see map in Fig. 3) occur within the Bucaramanga Nest (Prieto *et al.*, 2012; Poli *et al.*, 2016), and the rest correspond to the main-shock and aftershocks of the  $M_1$  6.0 Mesetas earthquake sequence (Servicio Geológico Colombiano [SGC], 2020). Example records of some of the earthquakes are shown in the supplemental material (Fig. S3a–c).

## Estimating the IMF

In this study, we use deconvolution interferometry (Snieder and Safak, 2006; Prieto *et al.*, 2010; Nakata *et al.*, 2013; Nakata and Snieder, 2014) for monitoring purposes. In applying deconvolution interferometry, we calculate the IRF:

$$D_n(z, z_0, t) = F^{-1} \left[ \frac{U_n(z, \omega) U_n^*(z_0, \omega)}{U_n^2(z_0, \omega)} \right], \quad (1)$$

using the multitaper algorithm (Prieto *et al.*, 2009) in which  $U_n(z, \omega)$  and  $U_n(z_0, \omega)$  represent the recorded ground acceleration at circular frequency  $\omega$  at floor levels  $z$  and  $z_0$ , respectively. In our study, we use the sensors at floors 2, 5, 8, 11, and 14 (ceiling) leading to a total of 25 IRFs from all floor combinations for each horizontal component (X and Y). We do not analyze the vertical component. The subscript  $n$  represents the time window used to calculate the IRF, which is always the same for both floor levels. For earthquake and ambient-vibration data, the time window varies as explained subsequently.

In the case of the earthquake-based IRFs, we take 100-s-long windows starting 10 s before the predicted arrival time of the Pwaves at the Crisanto building. Deconvolution interferometry (equation 1) is applied without a water level to each segment after signals are detrended. No temporal averaging is performed, so the individual earthquake IRFs are used for monitoring. The resulting IRFs for all 49 earthquakes and the average IRF are shown in Figure 4.

For the continuous ambient-vibration IRFs, the 225-day-long record is divided into 10-min-long segments and equation (1) is applied to the detrended signals (again without a

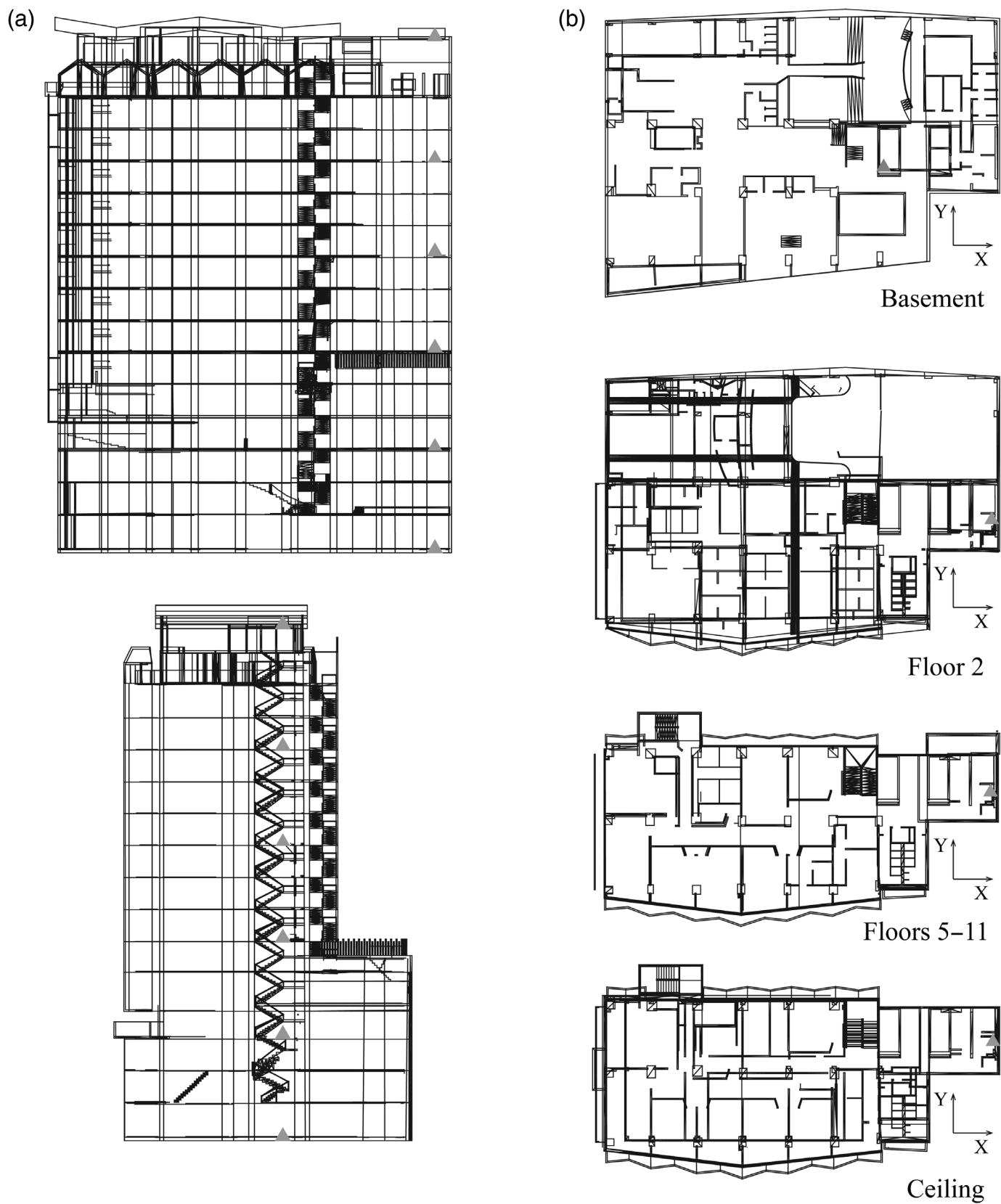
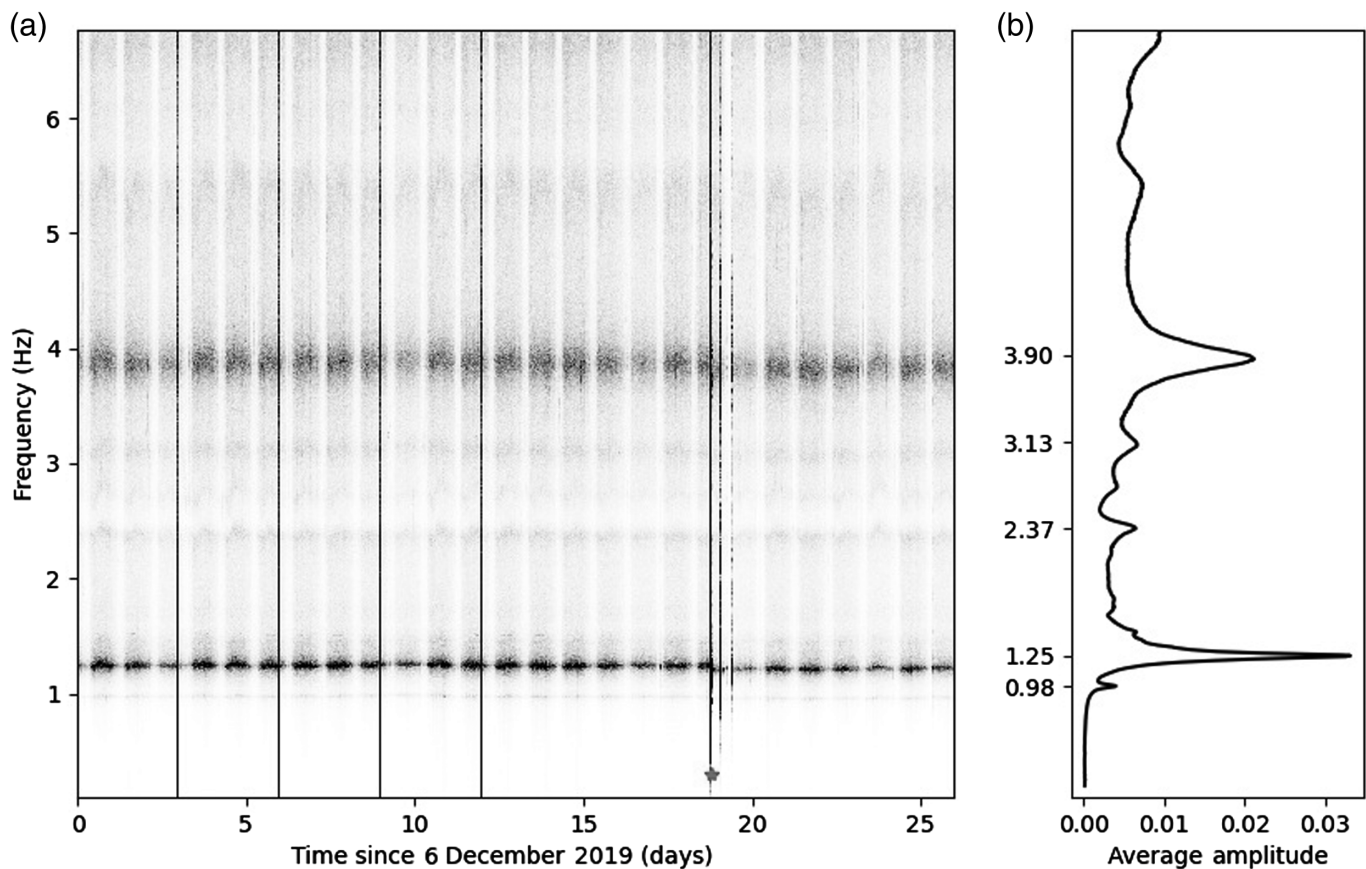


**Figure 1.** (a) Front view and (b) floor plan view of the Crisanto Luque building. ETNA-2 sensors on each floor are shown in gray triangles.



water level). In contrast to many studies in ambient seismic monitoring studies (e.g., Bensen *et al.*, 2007), we apply no amplitude normalization, and we do not remove windows with large amplitudes. To improve the coherent signal of the ambient-vibration data, we average the 10 min IRFs into 24 hr IRF stacks that are used for monitoring purposes. Figure 5 shows 70-day-long averaged IRFs based on ambient vibration, compared with the earthquake-based results.

We tested different processing parameters (window length, starting time, overlapping windows, and averaging length), but found that our results were not significantly affected and the conclusions of the work hold. Figures 4 and 5 show the resulting IRFs in which the wave pulse traveling upward and downward from the reference station can be clearly observed. The IRFs are also symmetric between negative and positive times.

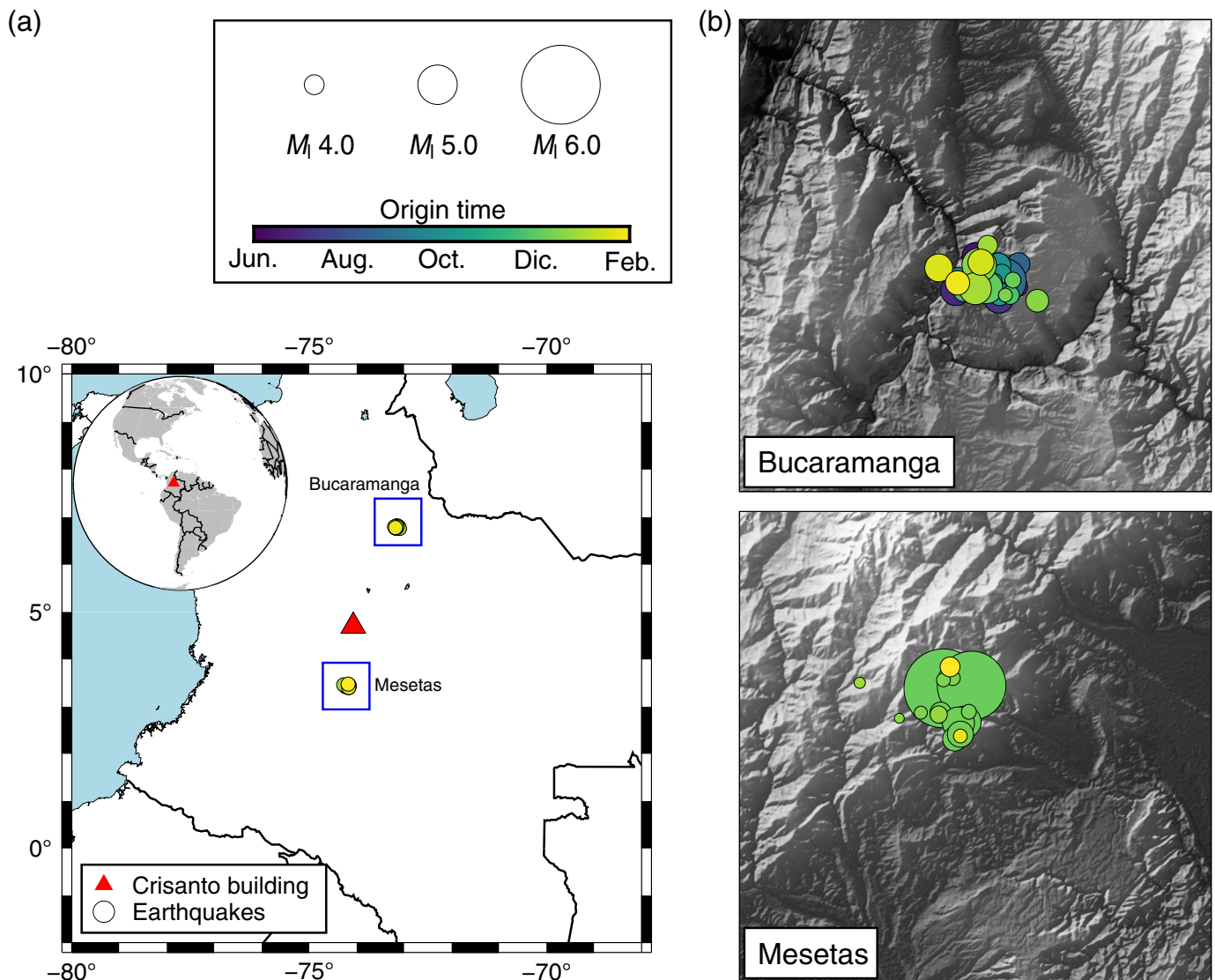
### Monitoring velocity variations

Velocity variations within an engineering structure may reflect changes in its internal characteristics such as spatial distribution or stiffness (Todorovska and Trifunac, 2008), opening and closing of existing cracks or formation of new cracks (Astorga *et al.*, 2018), and soil-structure interactions (Kohler *et al.*, 2007), so accurate estimates of wave propagation velocities are key. One way of estimating the speed of traveling waves using the IRF is by looking at the deconvolution with respect to the roof (Snieder and Safak, 2006; Prieto *et al.*, 2010; Rahmani and Todorovska, 2021) or with respect to other floors

**Figure 2.** (a) Amplitude spectrogram for ambient-vibration data for the X-component sensor located at the 14th floor and average spectral amplitudes. Star represents the origin time of the  $M_l$  6.0 Mesetas earthquake. (b) Average amplitude spectrum from (a) with approximate frequencies of peaks.

(Kohler *et al.*, 2007; Nakata *et al.*, 2013; Nakata and Snieder, 2014; Mordret *et al.*, 2017). Unfortunately, arrival times are based on detecting or picking the arrival of an upgoing or downgoing wave, and for small velocity variations (0%–10%), the arrival-time differences of direct phases are on the order of 10–30 ms, which can easily be below the resolution when comparing filtered IRFs. In addition, the limited number of sensors in the Crisanto building prevents clear tracking of the wave propagation of individual phases (Kohler *et al.*, 2007) or possible reflections within the building (Mordret *et al.*, 2017).

The estimated velocity of the X and Y-component is 200 and 250 m/s, respectively. Because we are focused on velocity variations, the absolute values of the wavespeeds are not necessary, and only relative velocity variations are studied. To estimate the relative velocity variations ( $dv/v$ ), we compare a current IRF at a given time  $t_0$  relative to a reference IRF by measuring relative phase shift (or time delays) along the two traces. In this study, we use as a reference IRF the 70 day average IRF (Fig. 5), the IRF for the 49 earthquake IRFs, or the daily stack IRF using ambient vibrations. The IRFs are similar to

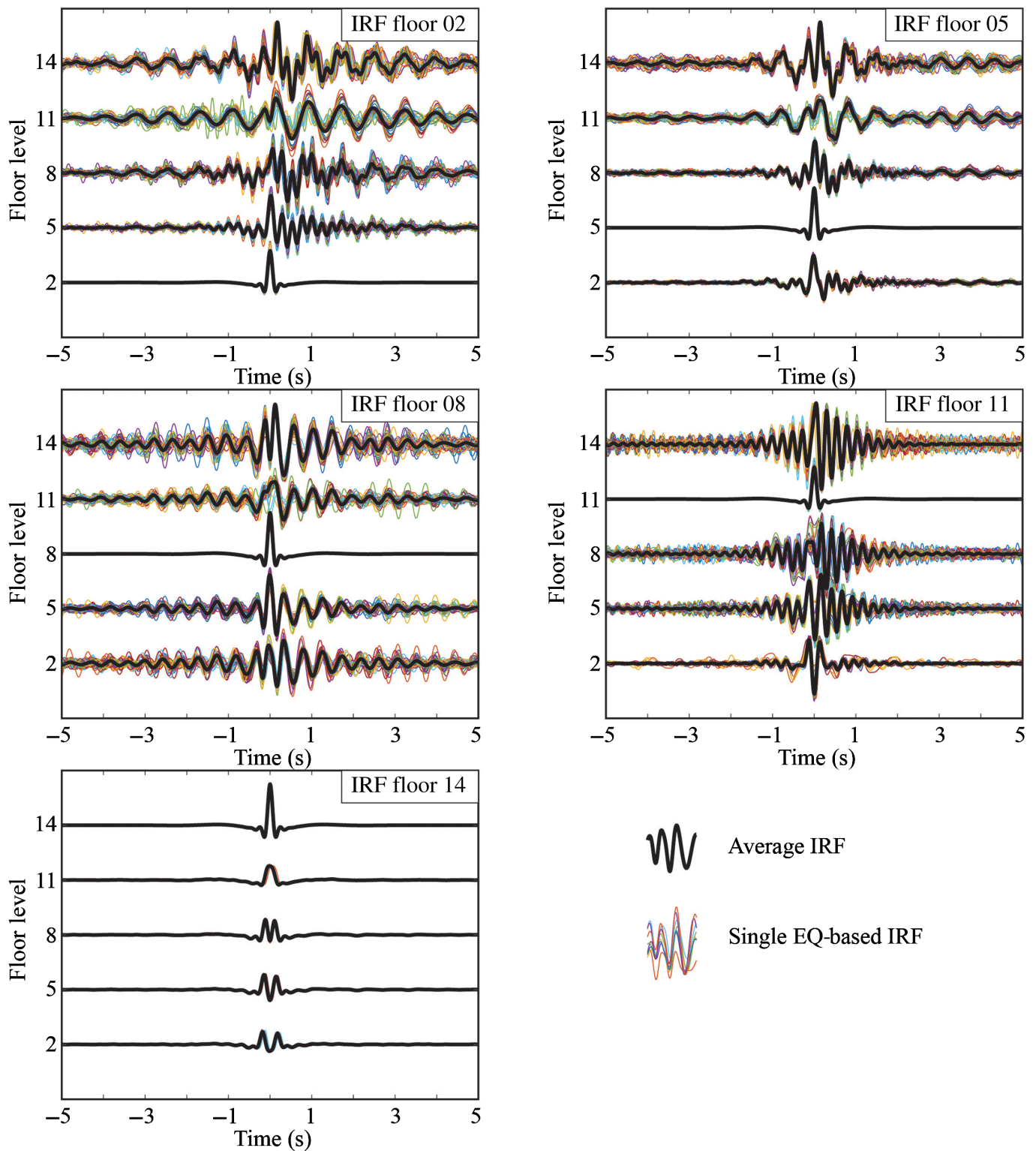


each other with small phase shifts at different time scales. A clear and symmetric phase shift is observed at Julian day 358 (the day of the  $M_l$  6.0 earthquake), which suggests a significant change of the building response (see Figs. S4, S5a–b; xample.g., IRFs at various floors and frequencies for the entire experiment).

To estimate the time delays, we use the stretching technique (Sens-Schönfelder and Wegler, 2006; Hadziioannou *et al.*, 2009). Under the assumptions of a small and uniform velocity change, the time shift between two waveforms is proportional to the travel time (Hadziioannou *et al.*, 2009). By stretching the time axis of one waveform and finding an optimal cross correlation with the other waveform, the stretching method can estimate a relative velocity change. Although other methods are available (Clarke *et al.*, 2011; Mikesell *et al.*, 2015; Jiang and Denolle, 2020), as pointed out by Mordret *et al.* (2017), the estimated errors using a moving window method were higher than the stretching method. Similar results were obtained regardless of the method using a small subset of the data.

**Figure 3.** (a) Location of building array (red triangle) and earthquakes used in this study (colored circles). Inset map shows the location of study area in South America. (b) Two source areas (Bucaramanga Nest and Mesetas earthquake). Earthquake parameters taken from the Servicio Geológico Colombiano 43 colored by origin time and size based on magnitude. The color version of this figure is available only in the electronic edition.

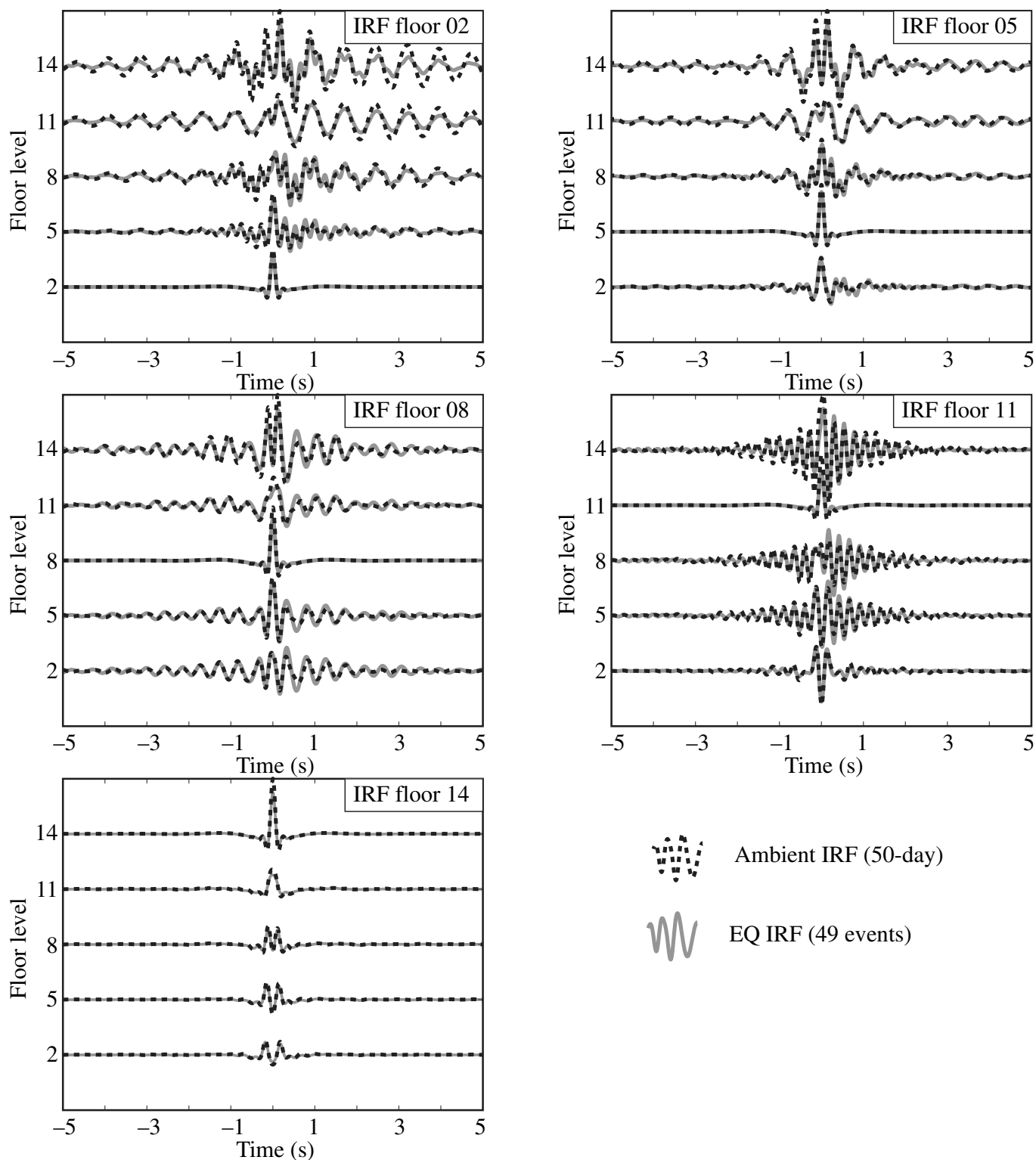
In applying the stretching method, we assume that a small velocity change occurs homogeneously within the building, so the IRF will be a stretched or compressed version of the reference IRF. We follow (Mordret *et al.*, 2017) to obtain an estimate of the velocity variation ( $dv/v$ ) by stretching the reference IRF over a certain range and cross correlating with the current IRF. The optimal stretching, and thus  $dv/v$ , is the one with the highest correlation coefficient (Fig. S6). We perform these  $dv/v$  estimates over different frequency bands to focus on the different modes of the building as shown in Figure 2. We perform a grid search between  $-20\%$  and  $20\%$  for the  $dv/v$  with 200 bins



and refine the search around the maximum correlation coefficient with another 200 bins.

To reduce the effect of the early arrivals in comparing the current and reference IRFs, we apply an automatic gain control to each IRF so that the cross correlation represents the similarity of the entire waveforms rather than the similarity of the early arrivals. In the following, we only use the  $dv/v$  estimates

**Figure 4.** Earthquake-based impulse response function (IRF) for the 49 earthquakes analyzed in this study (colored traces) and the average IRF (black traces) for all possible floor combinations. Reference floor is marked on each panel. IRFs are filtered between 0.5 and 5.0 Hz in these plots. The color version of this figure is available only in the electronic edition.



with correlation coefficients higher than 0.8. The length of the window used for phase delay and  $dv/v$  estimation depends on the frequency band of interest (see Table S2 for frequency bands and window lengths). We tested estimating the  $dv/v$  using only the positive or negative side of the IRFs with no significant change in the results.

**Figure 5.** Ambient-vibration-based IRF from the average of 70 days (black traces) for all possible floor combinations, compared with earthquake-based IRF (gray traces). Reference floor is marked on each panel. IRFs are filtered between 0.5 and 5.0 Hz in these plots.

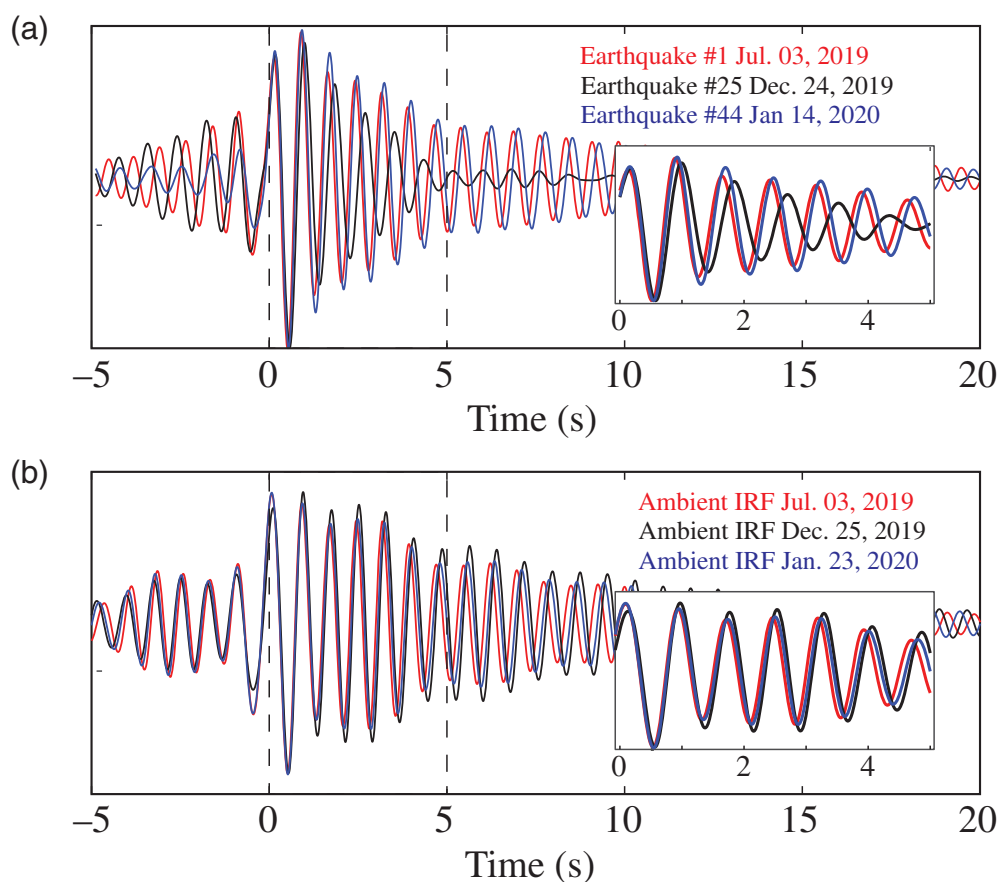


**Figure 6.** (a) Comparison of example IRF between second and eighth floors using earthquake and (b) ambient-vibration data filtered between 0.5 and 2.0 Hz. Inset shows IRFs in the first 5 s. Observable phase shifts are interpreted as velocity variations within the building. Note that the phase shift around the  $M_l$  6.0 Mesetas earthquake is largest (black trace) and a slight recovery is observed in 2020 (blue trace). The phase shift is more significant using earthquake-based IRFs. The color version of this figure is available only in the electronic edition.

### Velocity variation results

Figure 6 shows an example comparison of earthquake and ambient-vibration IRFs before, just after, and weeks after the Mesetas earthquake. Clear phase delays are observed after the mainshock, but it is notable that the phase delays are much more pronounced using the earthquake-based IRFs. This is confirmed using all of the available earthquake-based IRFs. Figure 7 shows the estimated velocity variations over the period of study, with a very significant velocity decrease of around 10% during the first few days after the Mesetas earthquake. Mordret *et al.* (2017) observed velocity variations on the order of 1%–2%, which they linked to weather conditions. In contrast, building responses after large earthquakes do show significant variations, estimated to about 20% for a building in Japan after the Tohoku earthquake (Nakata *et al.*, 2015; Wen and Kalkan, 2017; Nakata and Kashima, 2018).

Figure 8 shows the estimated velocity variations using the ambient-vibration IRFs for the X component. A similar pattern to what we observed using the earthquake data emerges; there

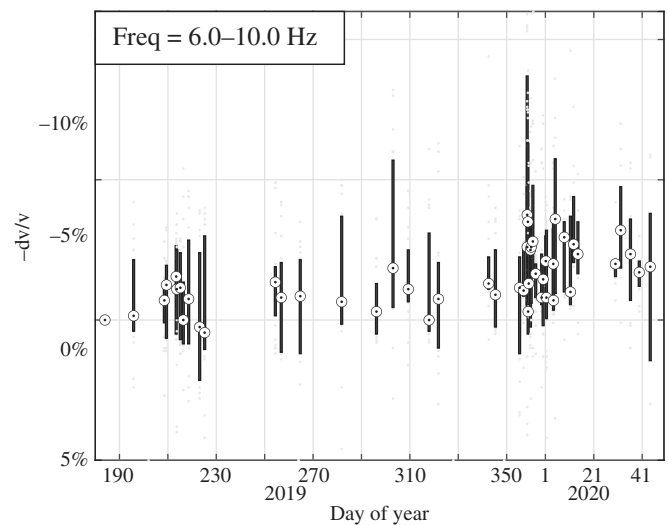
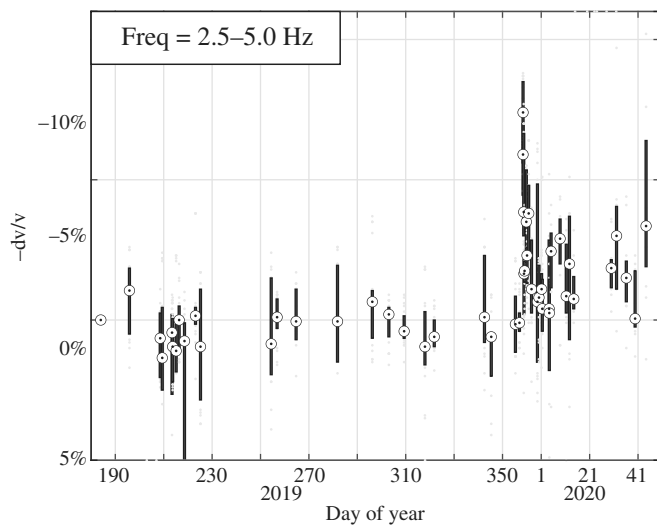
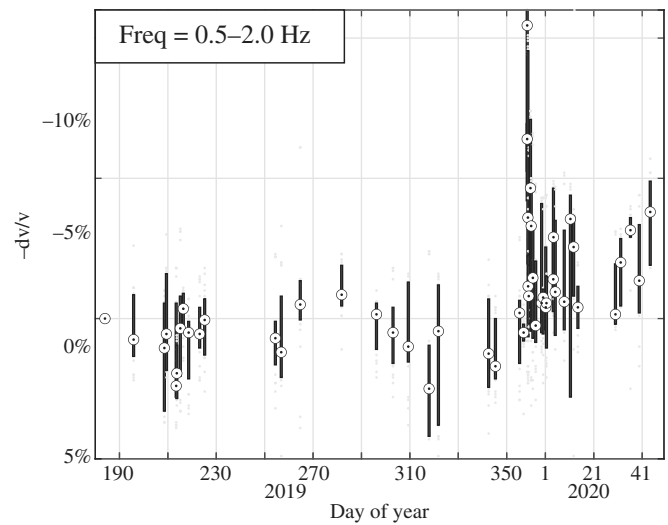
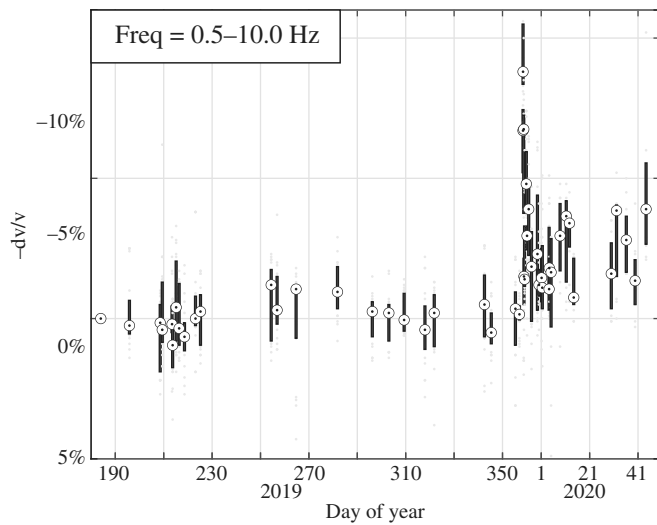
is a significant velocity change after the Mesetas earthquake. However, in contrast with the earthquake results, the amplitude of the velocity variation is only about 2%. The discrepancy is quite significant just after the mainshock, but after a few days, the earthquake-based velocity variations seem to show a recovery of the building response and suggest a velocity reduction of about 1%–2%, similar to what is observed using ambient vibrations. The ambient vibrations show a permanent velocity variation with no clear recovery. The ambient-vibration data used here represent a 24 hr average IRF, whereas the earthquake IRF is based on a 100 s window.

We argue that the sharp velocity decrease of 2% observed in Figure 8 is statistically significant. Both the median velocity variations from the 20 IRF combinations (we neglect the autodeconvolution) as well as the 25th and 75th percentiles (boxes) confirm the robust velocity drop. Figure S9 shows velocity varia-

tion using the ambient vibrations for the Y component. Although a similar pattern is observed for the Y component, the velocity variations at higher frequencies (6–10 Hz) shows large uncertainties.

### Discussion and Conclusions

Why are the amplitudes so different comparing the  $dv/v$  variations from ambient-vibration-based and earthquake-based IRFs? Why is the velocity variation showing a recovery using earthquake data and no such recovery using ambient vibrations? The spectrogram of the X component shown in Figure 2 may hold part of the answer. After the Mesetas earthquake, the fundamental mode (1.25 Hz) shows a clear shift that persists long after the mainshock (see Fig. S2 for a similar pattern for the Y component). Similar behavior seems to be observed also for the higher mode at 3.9 Hz. We speculate that this permanent mode shift is what the ambient vibration is detecting as a not-recovered velocity variation of about 2%. In contrast, the large velocity variations using earthquake data



may reflect a nonlinear response and more significant fundamental frequency variations of the building (Clinton *et al.*, 2006; Mikael *et al.*, 2013) due to strong shaking of the building. The observed recovery (Figs. 7 and 8) is not complete, and a remnant 1%–2% velocity reduction is still observed a few days after the mainshock. Because most of the recorded earthquakes are  $M_1$  4–5, shaking is not as strong and is similar to ambient-vibration data, thus really reflecting the average, linear response of the building with a 2% velocity reduction with respect to the building before the Mesetas earthquake. So, we believe  $dv/v \sim 2\%$  is an appropriate estimate of the long-term velocity change, whereas the 10% corresponds to the coseismic variation of the building (Wen and Kalkan, 2017; Astorga *et al.*, 2018).

Unfortunately, the building array did not continue to record after February 2020, and it is not clear whether the building response has recovered to its original condition or a velocity decrease was left due to the  $M_1$  6.0 Mesetas earthquake. A future visit and repeated experiment with the same sensors located in the same positions may allow us to answer this question.

Building monitoring can potentially be used continuously using either recorded ground motions due to earthquakes or

**Figure 7.** Seismic velocity variations from earthquake-based IRFs showing a 10% velocity reduction after the Mesetas earthquake (velocity reduction is up). A rapid recovery to about 1%–2% is observed. Median (white circle), mean (purple dot), individual estimates (gray dots), and 25% and 75% quantiles (boxes) from the 25 IRF station pairs at the X component of the Crisanto building at different frequency bands. We do not use the autodeconvolution for velocity variation analysis.

using ambient-vibration data that may include both anthropogenic and other natural sources. The relative velocity variations obtained using IRF phase delays provide very precise estimates and can detect changes associated with strong shaking. It is important to be aware of potential differences of ambient-vibration- and earthquake-based velocity variations that may be due to nonlinear response of the building and give very different velocity variations. In Figure 8 (and also evident in Fig. S4 as small kinks in peaks and troughs), small velocity variations are observed that are not only associated with the Mesetas or other earthquakes but also related to environmental conditions, but this is something we did not pursue in this work and hope to address in future work.

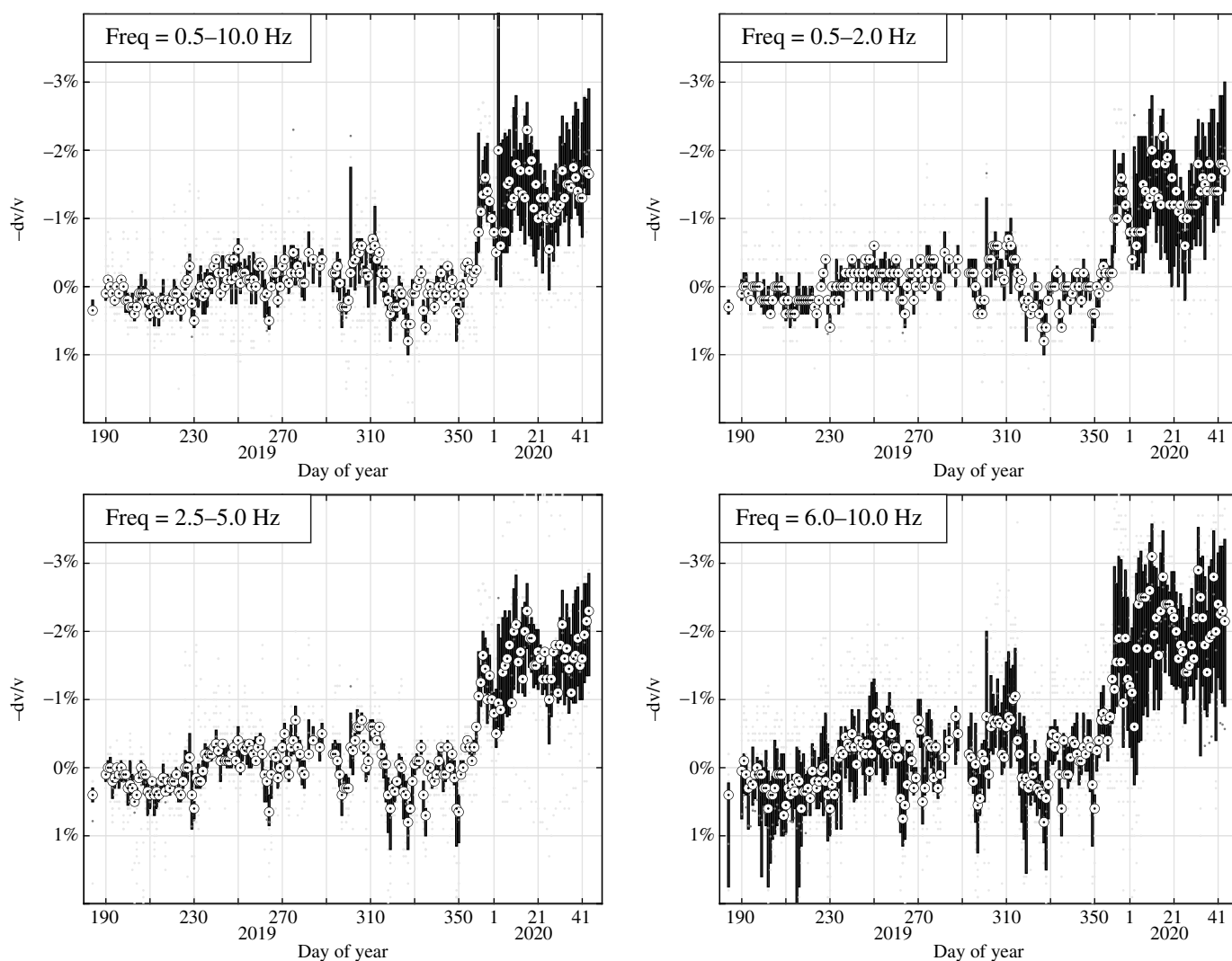


**Figure 8.** Seismic velocity variations from ambient-vibration-based IRFs showing a 2% order variation after the Mesetas earthquake (velocity reduction is up). In contrast to the earthquake-based results, no clear recovery is observed. Median (white circle), mean (purple dot), individual estimates (gray dots), and 25% and 75% quantiles (boxes) from the 25 IRF station pairs at the X component of the Crisanto building at different frequency bands.

Differences in velocity variations observed between low-amplitude ambient vibrations and large-amplitude earthquake shaking have been observed previously (e.g., [Wen and Kalkan, 2017](#)) and are interpreted as being due to nonstructural components affecting the stiffness of the structure during ambient measurements. [Astorga et al. \(2018\)](#) argue that the continuous damage process within the structure is sampled using ambient vibrations, whereas the larger amplitude motions, such as the Mesetas earthquake, can alter the degree of heterogeneities (cracks) and determines the nature of the quick recovery observed. A combination of both earthquake-based and ambient-vibration-based deconvolution interferometry provides a more complete picture of the state of health of engineering structures.

## Data and Resources

All data used in this work were collected as part of a project supported by ECCI. Data are available upon request to the authors. Authors will make every effort to upload the data to Incorporated Research Institutions for Seismology (IRIS) or other servers for any reader to download the data. The supplemental material includes additional

figures describing the data and results for the Y component. Tables include the list of earthquakes used for earthquake-based deconvolution and parameters used for velocity variation using the stretching method.

## Declaration of Competing Interests

The authors acknowledge that there are no conflicts of interest recorded.

## Acknowledgments

Special thanks to ECCI University for acquiring the sensors, performing the installation, and allowing the authors to use their data and to NetOps at ECCI, who provided the support for the development of this

pioneering project in Colombia. G. P. acknowledges the partial support from International Geoscience Programme (IGCP) Project 669.

## References

- Astorga, A., P. Guéguen, and T. Kashima (2018). Nonlinear elasticity observed in buildings during a long sequence of earthquakes, *Bull. Seismol. Soc. Am.* **108**, no. 3A, 1185–1198.
- Bensen, G. D., M. H. Ritzwoller, M. P. Barmin, A. L. Levshin, F. Lin, M. P. Moschetti, N. M. Shapiro, and Y. Yang (2007). Processing seismic ambient noise data to obtain reliable broad-band surface wave dispersion measurements, *Geophys. J. Int.* **169**, no. 3, 1239–1260.
- Brenguier, F., M. Campillo, C. Hadziioannou, N. Shapiro, R. Nadeau, and E. Larose (2008). Postseismic relaxation along the San Andreas fault at Parkfield from continuous seismological observations, *Science* **321**, 1478–1481.
- Brenguier, F., N. Shapiro, M. Campillo, V. Ferrazzini, Z. Duputel, O. Coutant, and A. Necessian (2008). Towards forecasting volcanic eruptions using seismic noise, *Nat. Geosci.* **1**, 126–130.
- Bukenya, P., P. Moyo, H. Beushausen, and C. Oosthuizen (2014). Health monitoring of concrete dams: A literature review, *J. Civil Struct. Health Monit.* **4**, 235–244.
- Cárdenas-Soto, M., H. Ramos-Saldaña, and M. Vidal-García (2016). Interferometría de ruido sísmico para la caracterización de la estructura de velocidad 3D de un talud en la 3ª Sección del Bosque de Chapultepec, *Bol. Soc. Geol. Mex.* **68**, no. 2, 173–186 (in Spanish).
- Çelebi, M. (2019). S<sup>2</sup>HM of buildings in United States, in *Seismic Structural Health Monitoring*, M. P. Limongelli and M. Çelebi (Editors), Springer, Cham, Switzerland, 3–30.
- Clarke, D., L. Zaccarelli, N. M. Shapiro, and F. Brenguier (2011). Assessment of resolution and accuracy of the moving window cross spectral technique for monitoring crustal temporal variations using ambient seismic noise, *Geophys. J. Int.* **186**, no. 2, 867–882.
- Clinton, J., S. Case Bradford, T. Heaton, and J. Favela (2006). The observed wander of the natural frequencies in a structure, *Bull. Seismol. Soc. Am.* **96**, no. 1, 237–257.
- Ebrahimian, M., and M. I. Todorovska (2015). Structural system identification of buildings by a wave method based on a nonuniform Timoshenko beam model, *J. Eng. Mech.* **141**, no. 8, 04015022, doi: [10.1061/\(ASCE\)EM.1943-7889.0000933](https://doi.org/10.1061/(ASCE)EM.1943-7889.0000933).
- Farrar, C. R., and K. Worden (2010). An introduction to structural health monitoring, *New Trends Vib. Based Struct. Health Monit.* **265**, no. 1851, 1–17.
- Hadziioannou, C., E. Larose, O. Coutant, P. Roux, and M. Campillo (2009). Stability of monitoring weak changes in multiply scattering media with ambient noise correlation: Laboratory experiments, *J. Acoust. Soc. Am.* **125**, no. 6, 3688–3695.
- Ikeda, T., and T. Tsuji (2018). Temporal change in seismic velocity associated with an offshore MW 5.9 Off-Mie earthquake in the Nankai subduction zone from ambient noise cross-correlation, *Prog. Earth Planet. Sci.* **5**, 1–12.
- Jiang, C., and M. Denolle (2020). NoisePy: A new high-performance python tool for ambient-noise seismology, *Seismol. Res. Lett.* **91**, no. 3, 1853–1866.
- Kaya, Y., and C. Ventura (2019). Seismic structural health monitoring of bridges in British Columbia, Canada, in *Seismic Structural Health Monitoring*, M. P. Limongelli and M. Çelebi (Editors), Springer, Cham, Switzerland, 31–49.
- Kohler, M., T. Heaton, and S. Bradford (2007). Propagating waves in the steel, moment-frame building recorded during earthquakes, *Bull. Seismol. Soc. Am.* **97**, no. 4, 1334–1345.
- Massari, A., R. Clayton, and M. Kohler (2018). Damage detection by template matching of scattered waves, *Bull. Seismol. Soc. Am.* **108**, no. 5A, 2556–2564, doi: [10.1785/0120170319](https://doi.org/10.1785/0120170319).
- Mikael, A., P. Gueguen, P. Y. Bard, P. Roux, and M. Langlais (2013). The analysis of long-term frequency and damping wandering in buildings using the Random Decrement Technique, *Bull. Seismol. Soc. Am.* **103**, no. 1, 236–246.
- Mikesell, T., A. Malcolm, D. Yang, and M. Haney (2015). A comparison of methods to estimate seismic phase delays: Numerical examples for coda wave interferometry, *Geophys. J. Int.* **202**, 347–360.
- Mordret, A., H. Sun, G. Prieto, M. Toksöz, and O. Büyükoztürk (2017). Continuous monitoring of high-rise buildings using seismic interferometry, *Bull. Seismol. Soc. Am.* **107**, no. 6, 2759–2773.
- Nakata, N., and T. Kashima (2018). Time-lapse changes in seismic response of building over 20 years due to earthquakes and aging, *Eleventh US National Conference on Earthquake Engineering*, Los Angeles, California, 25–29 June 2018.
- Nakata, N., and R. Snieder (2014). Monitoring a building using deconvolution interferometry. II: Ambient vibration analysis, *Bull. Seismol. Soc. Am.* **104**, no. 1, 204–213.
- Nakata, N., R. Snieder, S. Kuroda, S. Ito, T. Aizawa, and T. Kunimi (2013). Monitoring a building using deconvolution interferometry I: Earthquake-data analysis, *Bull. Seismol. Soc. Am.* **103**, no. 3, 1662–1678.
- Nakata, N., W. Tanaka, and Y. Oda (2015). Damage detection of a building caused by the 2011 Tohoku-Oki earthquake with seismic interferometry, *Bull. Seismol. Soc. Am.* **105**, no. 5, 2411–2419.
- Obermann, A., T. Planès, E. Larose, and M. Campillo (2013). Imaging preruptive and coeruptive structural and mechanical changes of a volcano with ambient seismic noise, *J. Geophys. Res.* **118**, 6285–6294.
- Oliveira, S., and A. Alegre (2019). Seismic and structural health monitoring of dams in Portugal, in *Seismic Structural Health Monitoring*, M. P. Limongelli and M. Çelebi (Editors), Springer, Cham, Switzerland, 87–113.
- Park, H., and B. Oh (2018). Damage detection of building structures under ambient excitation through the analysis of the relationship between the modal participation ratio and story stiffness, *J. Sound Vib.* **418**, 122–143.
- Planès, T., M. Mooney, J. Rittgers, M. Parekh, M. Behm, and R. Snieder (2016). Time-lapse monitoring of internal erosion in earthen dams and levees using ambient seismic noise, *Géotechnique* **66**, no. 4, 301–312.
- Poli, P., G. Prieto, C. Yu, M. Florez, H. Agurto-Detzel, T. Mikesell, G. Chen, V. Dionicio, and P. Pedraza (2016). Complex rupture of the M6.3 2015 March 10 Bucaramanga earthquake: Evidence of strong weakening process, *Geophys. J. Int.* **205**, 988–994.
- Prieto, G., G. Beroza, S. Barret, G. Lopez, and M. Florez (2012). Earthquake nests as natural laboratories for the study of intermediate-depth earthquake mechanics, *Tectonophysics* **570/571**, 42–56.
- Prieto, G., J. Lawrence, A. Chung, and M. Kohler (2010). Impulse response of civil structures from ambient noise analysis, *Bull. Seismol. Soc. Am.* **100**, no. 5A, 2322–2328.

- Prieto, G., R. Parker, and F. Vernon (2009). A Fortran 90 library for multitaper spectrum analysis, *Comput. Geosci.* **35**, 1701–1710.
- Rahmani, M., and M. I. Todorovska (2021). Structural health monitoring of a 32-storey steel-frame building using 50 years of seismic monitoring data, *Earthq. Eng. Struct. Dynam.* **50**, no. 6, 1777–1800, doi: [10.1002/eqe.3422](https://doi.org/10.1002/eqe.3422).
- Salvermoser, J., C. Hadziioannou, and S. Stähler (2015). Structural monitoring of a highway bridge using passive noise recordings from street traffic, *Acoust. Soc. Am.* **138**, no. 6, 3864–3872.
- Sens-Schönfelder, C., and U. Wegler (2006). Passive image interferometry and seasonal variations of seismic velocities at Merapi Volcano, Indonesia, *Geophys. Res. Lett.* **33**, L21302, doi: [10.1029/2006GL027797](https://doi.org/10.1029/2006GL027797).
- Servicio Geologico Colombiano (SGC) (2020). *El sismo de Mesetas—Meta del 24 de diciembre de 2019. Aspectos sismológicos, movimiento fuerte y consideraciones geodésicas. Informe Técnico*, Servicio Geologico Colombiano, Bogota, Colombia (in Spanish).
- Snieder, R., and E. Safak (2006). Extracting the building response using seismic interferometry: Theory and application to the Millikan library in Pasadena, California, *Bull. Seismol. Soc. Am.* **96**, no. 2, 586–598.
- Snieder, R., A. Gret, H. Douma, and J. Scales (2002). Coda wave interferometry for estimating nonlinear behavior in seismic velocity, *Science* **295**, 2253–2255.
- Snieder, R., M. Miyazawa, E. Slob, I. Vasconcelos, and K. Wapenaar (2009). A comparison of strategies for seismic interferometry, *Surv. Geophys.* **30**, 503–523.
- Sun, H., A. Mordret, G. Prieto, M. Toksöz, and O. Büyüköztürk (2017). Bayesian characterization of buildings using seismic interferometry on ambient vibrations, *Mech. Syst. Signal Process.* **85**, 468–486.
- Todorovska, M. I., and M. D. Trifunac (2008). Earthquake damage detection in the Imperial County Services Building III: Analysis of wave travel times via impulse response functions, *Soil Dynam. Earthq. Eng.* **28**, no. 5, 387–404.
- Wen, W., and E. Kalkan (2017). System identification based on deconvolution and cross-correlation—An application to a twenty-story instrumented building in Anchorage, Alaska, *Bull. Seismol. Soc. Am.* **107**, no. 2, 718–740.

---

Manuscript received 16 August 2021

Published online 22 December 2021